MicroDreamer: Zero-shot 3D Generation in ∼20 Seconds by Score-based Iterative Reconstruction

Luxi Chen[*1], **Zhengyi Wang**[*2], **Zihan Zhou**[1], **Tingting Gao**[3],
Hang Su[2], **Jun Zhu**[2], **Chongxuan Li**[†1]
[1]Gaoling School of Artificial Intelligence, Renmin University of China,
[2]Dept. of Comp. Sci. & Tech., BNRist Center, Tsinghua-Bosch Joint ML Center, Tsinghua University,
[3]Kuaishou Technology.

Abstract

Optimization-based approaches, such as score distillation sampling (SDS), show promise in zero-shot 3D generation but suffer from low efficiency, primarily due to the high number of function evaluations (NFEs) required for each sample. In this paper, we introduce score-based iterative reconstruction (SIR), an efficient and general algorithm mimicking a differentiable 3D reconstruction process to reduce the NFEs. Given a single set of images sampled from a multi-view score-based diffusion model, SIR repeatedly optimizes 3D parameters, unlike the single-step optimization in SDS. With other improvements in training, we present an efficient approach called MicroDreamer that generally applies to various 3D representations and 3D generation tasks. In particular, retaining a comparable performance, Micro-Dreamer is 5-20 times faster than SDS in generating neural radiance field and takes about 20 seconds to generate meshes from 3D Gaussian splatting on a single A100 GPU, halving the time of the fastest zero-shot baseline, DreamGaussian. Our code is available at `https://github.com/ML-GSAI/MicroDreamer`.

1 Introduction

Recently, optimization-based approaches [1, 2, 3, 4, 5, 6, 7, 8, 9, 10, 11, 12, 13] particularly score distillation sampling (SDS) [1, 2] have emerged as promising avenues for 3D generation based on text-to-image diffusion models [14, 15, 16, 17, 18, 19]. These approaches are appealing due to their minimal, or even zero reliance on 3D data, in contrast to the data-intensive requirements of feed-forward approaches [20, 21, 22, 23, 24, 25, 26, 27, 28, 29, 30, 31, 32, 33, 34]. This advantage is particularly significant given that 3D data are costly and scarce. Despite their promising capabilities, optimization-based approaches suffer from low efficiency due to the extensive number of function evaluations (NFEs), i.e. forward passes of the diffusion model, required for each 3D object generation.

In comparison, the multi-step reconstruction process of 3D representations that enable differentiable rendering, such as neural radiance field (NeRF) [35, 36] and 3D Gaussian splatting (3DGS) [37], produce 3D contents extremely fast because they do not involve large generative neural networks. However, such approaches rely on true 3D data (i.e. abundant real multi-view images like 100 in NeRF [35]), making it unfeasible to text-to-3D and image-to-3D generation tasks. There exist works [38, 39, 40, 41] for 3D generation attempt to generate multi-views first to reconstruct 3D object directly, while such methods may suffer from texture ambiguity [39] in generated views and are limited to specific 3D representations with a long reconstruction time (see Sec. 5 for comparison).

This paper introduces an efficient and general algorithm termed **score-based iterative reconstruction (SIR)** for zero-shot 3D generation inspiring from reconstruction and iterative optimization to address

---

*Equal contribution; †Corresponding authors.

Figure 1: **MicroDreamer** can generate high-quality meshes in about **20 seconds** on a single A100, built on a multi-view diffusion model **without additional 3D data**.

the computational issues in Sec. 3. Similar to SDS, SIR iteratively updates 3D parameters, leveraging a multi-view diffusion model without additional 3D data. However, in each iteration, SIR distinguishes itself by repeatedly optimizing 3D parameters given a set of images produced by the diffusion model, mimicking the efficient 3D reconstruction process to reduce the total NFEs (see Fig. 4). To obtain 3D-consistent and high-quality images as the ground truth for better reconstruction in each iteration, we carefully design a hybrid forward process and a sampling process to refine the images rendered from the 3D object optimized in the latest iteration.

We delve into critical components beyond the algorithm to ensure compatibility with SIR. The comprehensive system is named by **MicroDreamer**, highlighting its efficiency for 3D generation. As detailed in Sec. 4, we introduce an initialization strategy for 3D objects, an annealed time schedule for diffusion, additional losses on reference images for image-to-3D, and a refinement procedure for deriving high-quality meshes from 3DGS.

SIR and MicroDreamer are broadly applicable to both NeRF and 3DGS and both text-to-3D and image-to-3D tasks, as detailed in Sec. 5. Employing three widely adopted multi-view diffusion models [42, 43, 44], we systematically compare SIR and SDS for NeRF generation. Retaining a comparable performance, SIR can accelerate the generation process by **5 to 20 times**. Besides, MicroDreamer can efficiently produce 3DGS and further refine it into high-quality meshes, delivering consistent 3D meshes in about **20 seconds** on a single A100 GPU – about twice as fast as the most competitive optimization-based alternatives, DreamGaussian [9]. Remarkably, MicroDreamer is on par with speed compared to feed-forward methods trained on extensive 3D data, with a very competitive CLIP similarity [45, 9].

2 Background

We present background on 3D representations, diffusion models, multi-view diffusion models, and current optimization-based 3D generation methods.

2.1 3D representation

Neural radiance fields [35, 36] (NeRF) and 3D Gaussian splatting [37] (3DGS) have emerged as popular 3D representations. NeRF employs an MLP to predict the colors and density of the input
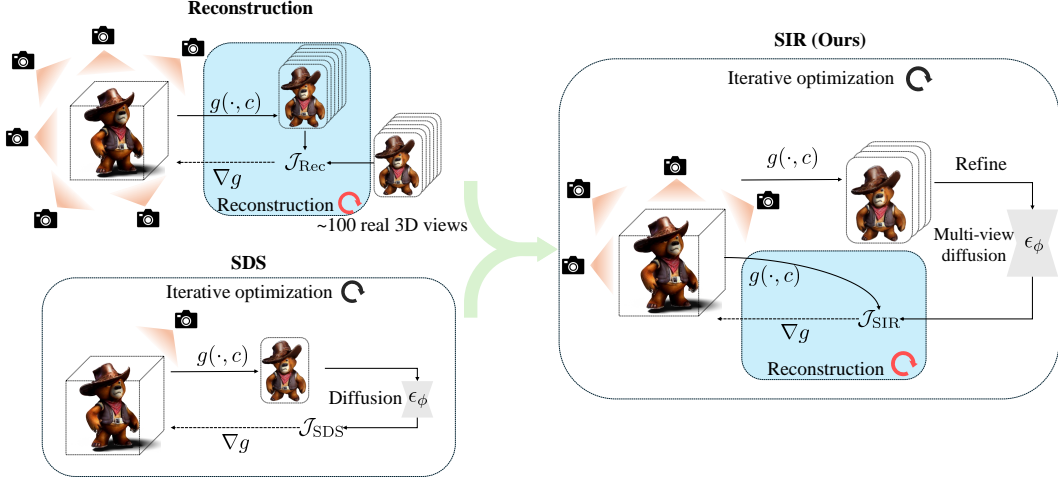
Figure 2: **Overview of SIR.** SIR is a zero-shot 3D generation method that marries the strengths of reconstruction and iterative optimization. SIR reutilizes the samples from diffusion multiple times through reconstruction, reducing the total NFEs and improving efficiency.

space coordinates. 3DGS consists of multiple 3D Gaussians parameterized by the colors, center, scale, and rotation quaternion. We denote the corresponding tunable parameters in both representations as θ. Given camera poses c, both approaches define a differentiable rendering process, denoted by $g(\theta, c)$. They are proven efficient and effective in 3D reconstruction [35, 37] and generation [1, 9].

2.2 Diffusion models

A diffusion model [14, 15, 16] consists of a forward process and a sampling process. The forward process gradually adds Gaussian noise to an input image from time 0 to T. For any $t \in (0, T)$, the noise-adding process can be written as follows:

$$x_t = \alpha_t x_0 + \sigma_t \epsilon := \text{Noise-adding}(x_0, 0 \to t), \quad \epsilon \in \mathcal{N}(0, I), \tag{1}$$

where the coefficients α_t and σ_t form the noise schedule of the diffusion model. A noise prediction network $\epsilon_\phi(x_t, t)$ with parameters ϕ is trained to predict the noise in the input x_t with the corresponding noise level, i.e. time t. Plugging in the noise prediction network into Eq. (1), we can solve x_0 from a noisy image x_t of time t by a single-step prediction as follows:

$$\hat{x}_0^t = \frac{1}{\alpha_t} x_t - \frac{\sigma_t}{\alpha_t} \epsilon_\phi(x_t, t), \tag{2}$$

which is an efficient approximation of the original input.

Instead of using Eq. (2) directly, the sampling process of diffusion gradually denoises through the noise prediction network and generates images from pure Gaussian noise. Among existing samplers [46, 47, 48, 49, 50, 51], the denoising diffusion implicit models (DDIM) [52] facilitate a sequence of samplers with random noise control η. When $\eta = 0$, it solves the equivalent probability flow ordinary differential equation (ODE) [16] of the diffusion model and enjoys a fast sampling process with fewer number of function evaluations (NFEs)[2]. In this setting, the one-step sampling of DDIM is given by:

$$x_{t-1} = \frac{\alpha_{t-1}}{\alpha_t} x_t + \left(\sigma_{t-1} - \frac{\alpha_{t-1}}{\alpha_t} \sigma_t \right) \epsilon_\phi(x_t, t) := \text{Sampler}(x_t, t \to t - 1). \tag{3}$$

We refer the readers to the original paper [52] for the formula of $\eta > 0$. For $\eta = 1$, it represents a standard SDE sampler [15], with a higher tolerance for mismatches in the distributions of latent variables [53, 54].

---

[2]Throughout the paper, we refer to the number of forward passes through ϵ_ϕ as NFEs.

Besides, when $\eta = 0$ there is an inverse process (called DDIM inversion) that maps the distribution of images to the same distributions of noisy images as in Eq. (1) but it can maintain the unique feature of an input image and reconstruct it accurately through the corresponding DDIM sampler in Eq. (3) (see Fig. 3a). The (one-step) DDIM inversion [52] is formulated as follows:

$$x_{t+1} = \frac{\alpha_{t+1}}{\alpha_t} x_t + \left(\sigma_{t+1} - \frac{\alpha_{t+1}}{\alpha_t} \sigma_t \right) \epsilon_\phi(x_t, t) := \text{Inversion}(x_t, t \to t+1). \qquad (4)$$

2.3 Multi-view diffusion models

After being trained on a modest amount of 3D data, diffusion models can generate 3D-consistent multi-view, known as multi-view diffusion models. Among them, MVDream [42] takes text inputs and outputs multi-view images consistent in 3D. In contrast, Zero-1-to-3 [6] and ImageDream [44] focus on the Image-to-3D task, taking an additional reference image as input. These models output new viewpoint images consistent with the reference image. This paper directly utilizes these pre-trained multi-view diffusion models without any further fine-tuning. For more details, please refer to the original papers and the source code in our supplementary materials. Notably, such multi-view diffusion models cannot provide a sufficient number of consistent multi-view images for 3D reconstruction directly, as shown in Fig. 7a. Given that the multi-view diffusion in [38, 39, 40, 41] often incorporate with additional 3D priors and do not align with our setting in Sec. 4, we choose not to employ them in this paper.

2.4 Optimization-based algorithms for 3D generation

Built upon (multi-view) diffusion models, optimization-based methods (see Sec. 6 for a review) aim to generate 3D content in a zero-shot manner. Among them, score distillation sampling (SDS) [1, 2] is the most representative and popular approach. Formally, denoting the rendered images as $x = g(\theta, c)$, SDS repeats adding noise to x according to Eq. (1) and updating the 3D parameters θ by

$$\nabla_\theta \mathcal{J}_{\text{SDS}}(x = g(\theta); \phi) := \mathbb{E}_t \left[w(t)(\epsilon_\phi(\alpha_t x + \sigma_t \epsilon, t) - \epsilon) \frac{\partial x}{\partial \theta} \right], \qquad (5)$$

where $w(t)$ is a fixed weighting function and we omit the dependency on the prompt y and camera c for simplicity. Notably, by reparameterization [4] according to Eq. (2), SDS has an equivalent data-prediction form:

$$\nabla_\theta \mathcal{J}_{\text{SDS}}(x = g(\theta); \phi) = \mathbb{E}_t \left[\frac{w(t)\alpha_t}{\sigma_t} (x - \hat{x}_0^t) \frac{\partial x}{\partial \theta} \right]. \qquad (6)$$

3 Score-based iterative reconstruction

We present the general framework of score-based iterative reconstruction (SIR), an efficient and versatile algorithm combining both the advantages of differentiable 3D reconstruction and optimization methods in Sec. 3.1. SIR capitalizes on the efficiency of 3D reconstruction and aims to minimize the number of function evaluations (NFEs) typically required by existing methods while ensuring comparable quality through iterations. For better reconstruction, we introduce a carefully designed diffusion-based process to produce refined multi-view images as ground truth in Sec. 3.2.

3.1 Mimicking 3D reconstruction to reduce the NFEs

Existing zero-shot 3D generation algorithms [1, 2, 4, 8] iteratively optimize the 3D parameters based on a 2D diffusion (see Eq. (5) for SDS as an example). Consequently, these methods necessitate high NFEs, presenting a critical challenge to computational efficiency.

Naturally, reutilizing the outcomes of diffusion for successive updates of the 3D object—mimicking the process of differentiable 3D reconstruction could substantially decrease the overall NFEs required. However, 3D reconstruction typically requires a sufficient number of consistently aligned multi-view images, which cannot be directly obtained from the current multi-view diffusion models [6, 42, 44, 43] (see Sec. 6 for a review and discussion). Therefore, similar to existing optimization-based methods, we introduce a reconstruction-based algorithm with multiple iterations of optimizing dubbed **score-based iterative reconstruction (SIR)**, detailed as follows.
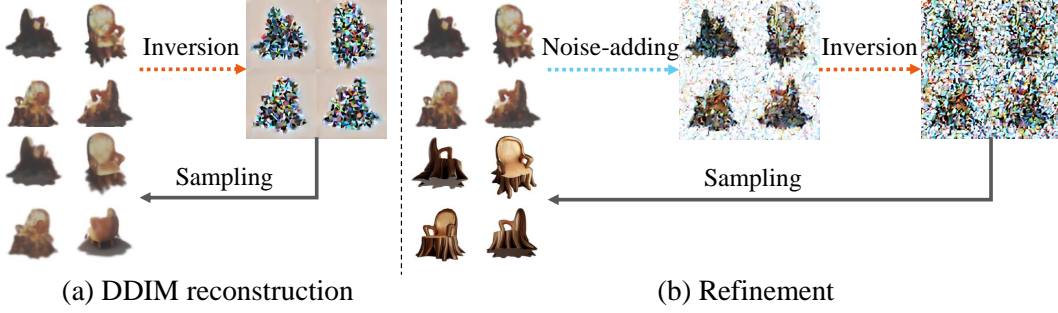
4

| (a) DDIM reconstruction | (b) Refinement |

Figure 3: **Overview of DDIM reconstruction and our refinement.** (a) The inversion process can preserve the 3D consistency of input images, and the input images can be recovered through the corresponding DDIM sampler. (b) After the carefully designed refinement of x by Eq. (9) and Eq. (10), the resulting $\hat{x}$ possesses enough high quality for 3D reconstruction.

Formally, SIR consists of K reconstruction iterations. In the k-th iteration, where $k = 0, 1, \ldots, K-1$, given initial 3D parameters $\theta_0^{(k)}$, we randomly select several camera poses $c^{(k)}$ (detailed in Sec. 4) and employ rendering function $g(\cdot, \cdot)$ to obtain multi-view images of the current 3D object as follows:

$$x^{(k)} = g(\theta_0^{(k)}, c^{(k)}). \tag{7}$$

For simplicity, let $x^{(k)}$ be a vector by flattening all images and concatenating them together and so do any subsequent set of multi-view images.

As detailed in Sec. 3.2, $x^{(k)}$ is then refined via a pre-trained multi-view diffusion model [42, 6, 44, 43]. The outcome, denoted as $\hat{x}^{(k)}$, serves as the ground truth for reconstruction in the current iteration. In particular, starting from $\theta_0^{(k)}$, keeping the camera poses $c^{(k)}$ unchanged, we optimize the 3D parameters w.r.t. the following reconstruction loss for $I^{(k)}$ steps:

$$\mathcal{J}_{\text{SIR}}(\theta; c^{(k)}, \hat{x}^{(k)}) = \|g(\theta, c^{(k)}) - \hat{x}^{(k)}\|, \tag{8}$$

where $\|\cdot\|$ can be any proper norm operator in principle while we choose ℓ_1 norm in our experiments. We use the final 3D parameters of the k-th iteration as the initialization of the next one, i.e. $\theta_0^{(k+1)} = \theta_{I^{(k)}}^{(k)}$ and outputs $\theta_0^{(K)}$ finally. See Sec. 4 for the initialization of the 0-th iteration, i.e. $\theta_0^{(0)}$.

Here we assume the rendered images and those sampled by the diffusion model are the same dimensional for simplicity. In Appendix B.1 we will further discuss how to deal with the latent diffusion model (LDM) [17]. Before that, we discuss how to obtain 3D-consistent and high quality $\hat{x}^{(k)}$ from $x^{(k)}$ for reconstruction in Sec. 3.2.

3.2 Refining multi-view images for reconstruction by diffusion

We treat $x^{(k)}$ as noise-free (i.e., at time 0 of the diffusion process) but low-quality images, refined by a forward process followed by a sampling process (see Fig. 3b).

The diffusion model has two equivalent forward processes [16]: the noise-adding process modeled by stochastic differential equations (SDEs) in Eq. (1) and the inversion process based on the probability flow ordinary differential equations (ODEs) in Eq. (4). In comparison, the noise-adding process is more efficient without function evaluation, and it aids in eliminating low-quality details through high-frequency noise. Conversely, the inversion process can preserve the 3D consistency and overall information of the current 3D object (see Fig. 3a). In addition, observations from existing experiments [55] indicate that diffusion models tend to generate details closer to time 0 and overall structure as they approach time T.

Inspired by this, we design a hybrid forward process that initially adds noise to time $t_1^{(k)}$ and then perform DDIM inversion to time $t_2^{(k)}$, where $t_1^{(k)} \in (0, T)$ and $t_2^{(k)} \in [t_1^{(k)}, T)$ are hyperparameters[3].

---

[3]Note that if $t_1^{(k)} = t_2^{(k)}$, the process is purely adding noise.

Algorithm 1: Score-based iterative reconstruction

---

1 **Input:** The number of iterations K, an initial 3D object $\theta_0^{(0)}$, a set of reconstruction steps
    $\{I^{(k)}\}_{k=0}^{K-1}$ and a set of camera poses $\{c^{(k)}\}_{k=0}^{K-1}$.

2 **Output:** A final 3D content $\theta_0^{(K)}$.

3 **for** k *from* 0 *to* $K-1$ **do**

4   Render N images $x^{(k)} = g(\theta_0^{(k)}, c^{(k)})$;

5   Obtain noisy $\tilde{x}^{(k)}$ from forward process for $x^{(k)}$ using Eq. (9);

6   Obtain refined $\hat{x}^{(k)}$ from sampling process for $\tilde{x}^{(k)}$ using Eq. (10);

7   **for** i *from* 0 *to* $I^{(k)} - 1$ **do**

8   Compute loss $L = \|g(\theta, c^{(k)}) - \hat{x}^{(k)}\|$ using Eq. (8);

9   Compute the gradient ∇L, update $\theta_i^{(k)}$ to $\theta_{i+1}^{(k)}$;

10   **end**

11   Obtain $\theta_0^{(k+1)} = \theta_{I^{(k)}}^{(k)}$.

12 **end**

In contrast to random sampled $t_2^{(k)}$ in existing algorithms including SDS [1], we adopt a linearly decreased schedule for $t_2^{(k)}$ as k progresses, detailed in Sec. 4. Formally, the process is defined as:

$$\tilde{x}^{(k)} = \text{Inversion}(\text{Noise-adding}(x^{(k)}, 0 \to t_1^{(k)}), t_1^{(k)} \to t_2^{(k)}), \tag{9}$$

where Noise-adding$(\cdot)$ is defined in Eq. (1) and Inversion$(\cdot)$ is defined in Eq. (4). The ablation in Fig. 7d shows the effectiveness of our hybrid forward process.

Note that generally $x^{(k)}$ does not follow the model distribution defined by the diffusion and the resulting $\tilde{x}^{(k)}$ do not strictly adhere to the marginal distribution at the corresponding time. Nevertheless, we still use existing sampling algorithms to obtain refined images $\hat{x}^{(k)}$ from $\tilde{x}^{(k)}$ as follows:

$$\hat{x}^{(k)} = \text{Sampler}(\tilde{x}^{(k)}, t_2^{(k)} \to 0). \tag{10}$$

Although other advanced sampling methods [46, 47, 48, 49, 50, 51] exist, we choose the popular DDIM in Eq. (3) and tune its noise hyperparameter η. The optimal value of η depends on the base model and we search for the best one in $\{0, 0.5, 1\}$ as detailed in Tab. 1 in Appendix A.

The whole process of SIR is presented in Algorithm 1. Compared with existing generation methods such as SDS, SIR benefits from reconstruction, i.e. leverages several NFEs for multiple updates of 3D parameters, and lowers the NFEs in total (see Fig. 4).

4 MicroDreamer

In addition to our algorithm SIR, we carefully analyze and design other critical elements in the 3D training and diffusion. Our comprehensive system is called **MicroDreamer** to highlight its efficiency.

3D initialization and camera views.   We utilize a direct reconstruction approach to initialize the 3D content. Specifically, we optimize the loss function in Eq. (8) by several steps (see Tab. 1 in Appendix A for detailed values) to update the 3D parameter, where $\hat{x}$ represents the images sampled from random noise via the pre-trained multi-view diffusion model. The camera views are uniformly sampled following the corresponding baselines [9, 56] except that the azimuth angles of different views in the same iteration are evenly distributed. In this setting, we are unable to directly utilize the diffusion model in [38, 39, 40] due to their fixed camera views conditioned generation.

Annealed time schedule.   We utilize an annealed time schedule $\{t_2^{(k)}\}_{k=0}^{K-1}$ for the end of the forward process. Intuitively, as the quality of the 3D assets improves, the input x in Eq. (7) becomes more proximate to the model distribution, thus requiring fewer steps to refine. This differs from SDS, which samples uniformly random t_2. Our preliminary experiments in Fig. 7c suggest that a linearly annealed schedule is sufficient. The endpoints of the schedule depend on the diffusion model, detailed in Tab. 1 in Appendix A. See Appendix C for the schedule of t_1.
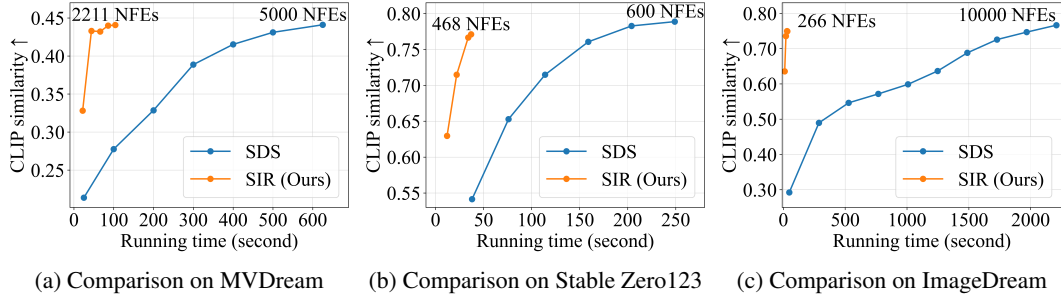
Figure 4: **Comparison of SIR and SDS on NeRF.** The change of the CLIP similarity in the generation process and final NFEs on different models. SIR achieves a 5-20 times acceleration and lowers NFEs.

Reference image loss for image-to-3D.   A reference image is available in image-to-3D, which is regarded as the ground truth front view of the 3D object on Stable Zero123 [6, 43] following DreamGaussian [9]. In this way, we add the reference loss in the same form as the reconstruction loss with Eq. (8) in each iteration of training. The weight set for the reference loss can be seen in Tab. 1.

3DGS settings and mesh refinement.   For simplicity, our approach on 3DGS largely adheres to the settings in DreamGaussian [9] unless specified. We incorporate a densify and prune procedure at every 50 updates during the initial 200 updates. We follow the mesh extraction method in DreamGaussian [9] and employ a threshold value of 0.2 in the marching cube algorithm [57, 9]. We utilize SIR to optimize the exported mesh texture in 3 iterations, with 15 steps per iteration, and we use a noise-adding process and DDIM with $\eta = 0$ for simplicity.

5   Experiment

We present the results on NeRF, 3DGS, and ablation sequentially. For a fair comparison, we utilize the widely used CLIP similarity [45] for quantitative comparison following DreamGaussian [9]. We consider 8 views at 0 elevation and evenly distributed in azimuth angles starting from 0. For all methods, the corresponding images are rendered from NeRF in Sec. 5.1 and mesh in Sec. 5.2. We report the average CLIP similarities between these images and the reference image or text. See Appendix D for details of the checkpoint and codebase.

5.1   Results on NeRF

We apply SIR algorithm on NeRF [35, 36, 56] leveraging three multi-view diffusion model from MVDream [42], Stable Zero123 [43, 6], and ImageDream [44]. For each model, we selected 6 input prompts from a widely used codebase [56] for testing, calculated NFEs, and recorded the change of the average CLIP similarity during the generation process. Compared with SDS, SIR lowers the total NFEs while generating a 3D object and can accelerate the generation process 5-20 times, as shown in Fig. 4. Besides, SIR can generate NeRF of high visual quality, as detailed shown in Appendix E, and the conclusion agrees with the results in Fig. 4.

5.2   Results on 3D Gaussian splatting

Qualitative comparisons.   We show the generated 3D meshes between the fastest optimization-based baseline DreamGaussian [9] and ours in Fig. 5. MicroDreamer halves the generation time of DreamGaussian while retaining competitive performance. We provide more visualization results of our methods in Appendix E.

Quantitative comparisons.   We compare MicroDreamer with seven competitive baselines including Point-E [24], Shap-E [23], One-2-3-45 [31], TriplanceGaussian [33], Wonder3D [39], LGM [30] and DreamGaussian [9]. We record the optimization time [4] for each model on a single NVIDIA A100 (80GB) GPU, and compute the average CLIP similarity for mesh on a test dataset consisting

---

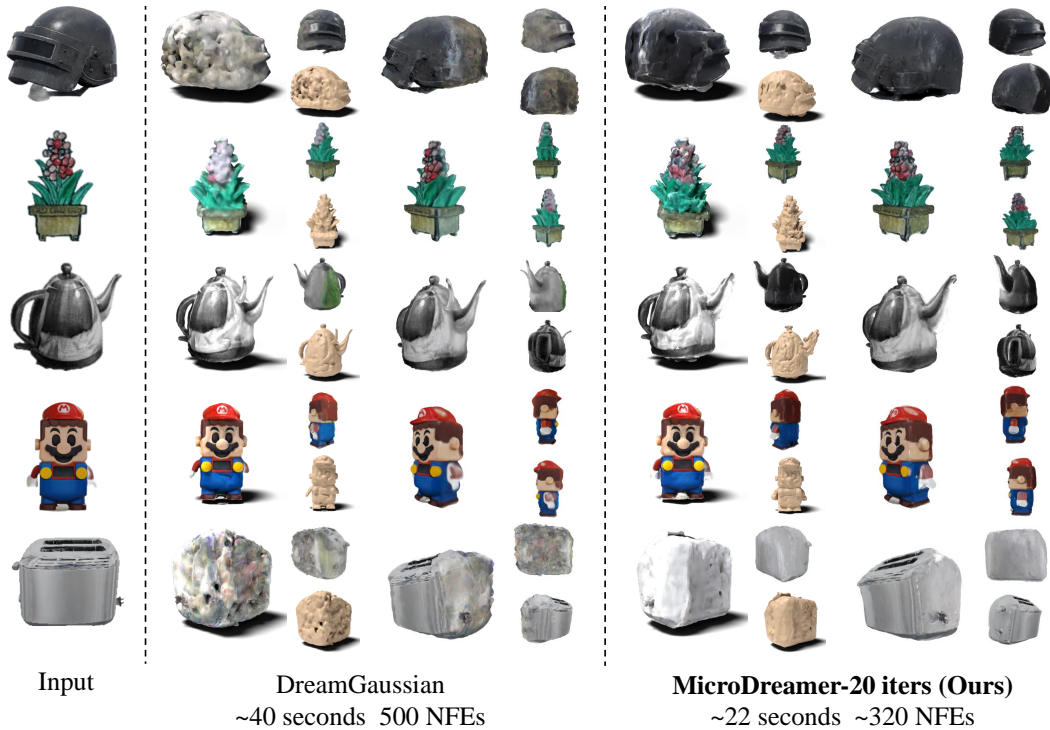[4]The detailed time recording method is provided in Appendix D.

Figure 5: **Qualitative comparisons on mesh from 3DGS.** MicroDreamer retains a comparable performance in terms of the visual quality of the mesh with higher efficiency.
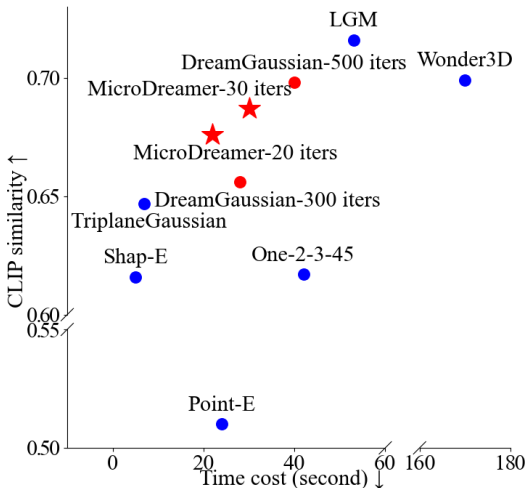

Figure 6: **Quantitative comparisons.** Our MicroDreamer achieves an excellent efficiency-effectiveness balance in terms of CLIP similarity. The zero-shot methods are highlighted in red.
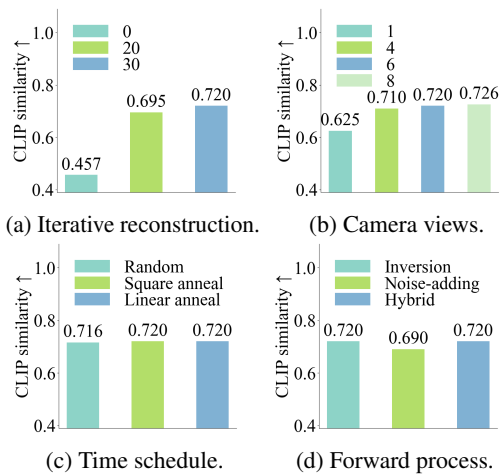
Figure 7: **Ablation study.** (a) Iterative reconstruction is necessary. (b) More camera views benefit. (c) A linear schedule is sufficient. (d) A hybrid forward process can be effective.

of 87 images collected from previous works [31, 38, 9], as shown in Fig. 6. As a zero-shot method, MicroDreamer is on par with speed compared to feed-forward methods, faster than DreamGaussian, with a very competitive CLIP similarity. We provide the time record and detailed tables in Appendix F. Notably, the sample quality of MicroDreamer can be improved as the multi-view diffusion evolves. See detailed limitations and future work in Sec. 7 and Appendix E.

8

5.3 Ablation study

Ablation on iterative reconstruction. Fig. 7a shows the necessity of iterative reconstruction. The case of $K = 0$ outputs our 3D initialization, which is reconstructed by a single process from images generated by random noise. Although increasing K improves quality, we set $K \leq 30$ for efficiency.

Ablation on number of camera poses. SIR necessitates more than 1 camera pose for reconstruction, as shown in Fig. 7b. The performance increases with more camera poses. We choose 6 on 3DGS with Stable Zero123 [43] model to balance efficiency and quality. See Tab. 1 for values in other settings.

Ablation on time schedule. We compare our linear schedule, the random schedule employed in SDS [1], and a square schedule with $t_2^{(k)} = (\frac{k}{K})^2 \cdot (0.8T - 0.2T) + 0.2T$. As shown in Fig. 7c, the schedules perform similarly. For simplicity and efficiency, we use the linear schedule by default.

Ablation on forward process. Fig. 7d compares three forward processes on 3DGS with the Stable Zero123 [43] model. The hybrid strategy performs better than noise-adding and is more efficient than inversion as discussed in Sec. 3.2. See Tab. 1 in Appendix A for other settings.

6   Related work

Optimization-based 3D generation. Built upon text-to-image diffusion models, optimization-based approaches [1, 2, 3, 4, 5, 6, 7, 8, 9, 10, 11, 12, 13, 58, 59, 60] usually generate 3D objects without additional 3D data. Among them, the most relevant line of work [1, 8, 10, 4, 2] proposes various distillation algorithms. Besides SDS [1], ProlificDreamer [8] proposes variational score distillation (VSD) to produce high-fidelity 3D objects via variational inference. LucidDreamer [10] incorporates DDIM inversion to strengthen the forward process. Though promising, such methods suffer from inefficiency problems due to large NFEs. Distinct from existing algorithms, SIR mimics 3D reconstruction processes to optimize the 3D parameters multiple times given a set of images produced by diffusion. Our experiments demonstrate that SIR is 5-20 times faster than SDS [1] on NeRF and twice as fast as the most competitive baseline DreamGaussian [9] on meshes.

Feed-forward 3D generation. Contrary to optimization-based methods, feed-forward methods [20, 21, 22, 23, 24, 25, 26, 27, 28, 61, 29, 31, 32, 33, 34, 62, 63, 64, 65] elect to use large-scale 3D datasets [66, 67] training to achieve a process that can directly generate 3D objects. Early methods are characterized by their speed but often produce lower-quality 3D structures with simple textures. Several recent methods, utilizing more data, have exhibited possibilities. Large reconstruction model (LRM) [68, 26] demonstrates the feasibility of training a Transformer to achieve a NeRF from a single image. Instant3D [69] further expands on LRM enabling it to accept multi-view input and reconstruct it into a NeRF. Remarkably, MicroDreamer is on par with speed compared to such methods trained on extensive 3D data, with a very competitive 3D quality measured by CLIP similarity [45, 9].

Multi-view prediction based 3D generation. There is also a line of work [38, 39, 40, 41] dedicated to enhancing the output of multi-view diffusion models by training on 3D datasets to reconstruct 3D objects using a single reconstruction process without iteration. These methods like Wonder3D[39] typically rely on 3D prior knowledge and are limited to specific 3D representations with a long reconstruction time. In contrast, thanks to the iterative process in SIR, MicroDreamer applies to various 3D representations and is more efficient (see Fig. 6 for a direct comparison).

7   Conclusion

We introduce SIR, an efficient and general algorithm combining both the strengths of 3D reconstruction and iterative optimization to reduce total NFEs in zero-shot 3D generation. SIR achieves a 5 to 20 times speed increase for NeRF generation compared to SDS. Remarkably, MicroDreamer generates high-quality meshes from 3DGS in about 20 seconds, outpacing the fastest zero-shot methods and matching the speed of feed-forward approaches with a competitive generation quality.

Limitations and broader impact. There is potential for further improving MicroDreamer's efficiency via employing consistency models [70, 71] or alternative sampling models that require fewer steps [72, 73]. Additionally, the fidelity and 3D consistency of the objects produced by MicroDreamer are directly limited by the quality of the outputs from multi-view diffusion. Nevertheless, we believe SIR is promising and may inspire future work as the multi-view diffusion evolves. Also, Micro-Dreamer can provide convenience for artists to create 3D assets. However, as a generative approach, our method may also be used for fabricating data and news, which warrants careful consideration.

8 Acknowledgement

References

[1] B. Poole, A. Jain, J. T. Barron, and B. Mildenhall, "Dreamfusion: Text-to-3d using 2d diffusion," *arXiv preprint arXiv:2209.14988*, 2022.

[2] H. Wang, X. Du, J. Li, R. A. Yeh, and G. Shakhnarovich, "Score jacobian chaining: Lifting pretrained 2d diffusion models for 3d generation," in *CVPR*, 2023, pp. 12 619–12 629.

[3] C.-H. Lin, J. Gao, L. Tang, T. Takikawa, X. Zeng, X. Huang, K. Kreis, S. Fidler, M.-Y. Liu, and T.-Y. Lin, "Magic3d: High-resolution text-to-3d content creation," *arXiv preprint arXiv:2211.10440*, 2022.

[4] J. Zhu and P. Zhuang, "Hifa: High-fidelity text-to-3d with advanced diffusion guidance," *arXiv preprint arXiv:2305.18766*, 2023.

[5] R. Chen, Y. Chen, N. Jiao, and K. Jia, "Fantasia3d: Disentangling geometry and appearance for high-quality text-to-3d content creation," *arXiv preprint arXiv:2303.13873*, 2023.

[6] R. Liu, R. Wu, B. V. Hoorick, P. Tokmakov, S. Zakharov, and C. Vondrick, "Zero-1-to-3: Zero-shot one image to 3d object," 2023.

[7] R. Shi, H. Chen, Z. Zhang, M. Liu, C. Xu, X. Wei, L. Chen, C. Zeng, and H. Su, "Zero123++: a single image to consistent multi-view diffusion base model," 2023.

[8] Z. Wang, C. Lu, Y. Wang, F. Bao, C. Li, H. Su, and J. Zhu, "Prolificdreamer: High-fidelity and diverse text-to-3d generation with variational score distillation," *Advances in Neural Information Processing Systems*, vol. 36, 2024.

[9] J. Tang, J. Ren, H. Zhou, Z. Liu, and G. Zeng, "Dreamgaussian: Generative gaussian splatting for efficient 3d content creation," *arXiv preprint arXiv:2309.16653*, 2023.

[10] Y. Liang, X. Yang, J. Lin, H. Li, X. Xu, and Y. Chen, "Luciddreamer: Towards high-fidelity text-to-3d generation via interval score matching," *arXiv preprint arXiv:2311.11284*, 2023.

[11] J. Sun, B. Zhang, R. Shao, L. Wang, W. Liu, Z. Xie, and Y. Liu, "Dreamcraft3d: Hierarchical 3d generation with bootstrapped diffusion prior," *arXiv preprint arXiv:2310.16818*, 2023.

[12] G. Metzer, E. Richardson, O. Patashnik, R. Giryes, and D. Cohen-Or, "Latent-nerf for shape-guided generation of 3d shapes and textures," *arXiv preprint arXiv:2211.07600*, 2022.

[13] T. Yi, J. Fang, G. Wu, L. Xie, X. Zhang, W. Liu, Q. Tian, and X. Wang, "Gaussiandreamer: Fast generation from text to 3d gaussian splatting with point cloud priors," *arXiv preprint arXiv:2310.08529*, 2023.

[14] J. Sohl-Dickstein, E. Weiss, N. Maheswaranathan, and S. Ganguli, "Deep unsupervised learning using nonequilibrium thermodynamics," in *International Conference on Machine Learning*. PMLR, 2015, pp. 2256–2265.

[15] J. Ho, A. Jain, and P. Abbeel, "Denoising diffusion probabilistic models," *Advances in Neural Information Processing Systems*, vol. 33, pp. 6840–6851, 2020.

[16] Y. Song, J. Sohl-Dickstein, D. P. Kingma, A. Kumar, S. Ermon, and B. Poole, "Score-based generative modeling through stochastic differential equations," 2021.

[17] R. Rombach, A. Blattmann, D. Lorenz, P. Esser, and B. Ommer, "High-resolution image synthesis with latent diffusion models," in *Proceedings of the IEEE/CVF Conference on Computer Vision and Pattern Recognition*, 2022, pp. 10 684–10 695.

[18] C. Saharia, W. Chan, S. Saxena, L. Li, J. Whang, E. Denton, S. K. S. Ghasemipour, B. K. Ayan, S. S. Mahdavi, R. G. Lopes *et al.*, "Photorealistic text-to-image diffusion models with deep language understanding," *arXiv preprint arXiv:2205.11487*, 2022.

[19] A. Ramesh, P. Dhariwal, A. Nichol, C. Chu, and M. Chen, "Hierarchical text-conditional image generation with clip latents," *arXiv preprint arXiv:2204.06125*, 2022.

[20] Z. Cao, F. Hong, T. Wu, L. Pan, and Z. Liu, "Large-vocabulary 3d diffusion model with transformer," *arXiv preprint arXiv:2309.07920*, 2023.

[21] H. Chen, J. Gu, A. Chen, W. Tian, Z. Tu, L. Liu, and H. Su, "Single-stage diffusion nerf: A unified approach to 3d generation and reconstruction," *arXiv preprint arXiv:2304.06714*, 2023.

[22] Z. Chen, F. Hong, H. Mei, G. Wang, L. Yang, and Z. Liu, "Primdiffusion: Volumetric primitives diffusion for 3d human generation," *arXiv preprint arXiv:2312.04559*, 2023.

[23] H. Jun and A. Nichol, "Shap-e: Generating conditional 3d implicit functions," *arXiv preprint arXiv:2305.02463*, 2023.

[24] A. Nichol, H. Jun, P. Dhariwal, P. Mishkin, and M. Chen, "Point-e: A system for generating 3d point clouds from complex prompts," *arXiv preprint arXiv:2212.08751*, 2022.

[25] Z. Liu, Y. Feng, M. J. Black, D. Nowrouzezahrai, L. Paull, and W. Liu, "Meshdiffusion: Score-based generative 3d mesh modeling," *arXiv preprint arXiv:2303.08133*, 2023.

[26] Y. Hong, K. Zhang, J. Gu, S. Bi, Y. Zhou, D. Liu, F. Liu, K. Sunkavalli, T. Bui, and H. Tan, "Lrm: Large reconstruction model for single image to 3d," *arXiv preprint arXiv:2311.04400*, 2023.

[27] N. Müller, Y. Siddiqui, L. Porzi, S. R. Bulo, P. Kontschieder, and M. Nießner, "Diffrf: Rendering-guided 3d radiance field diffusion," in *CVPR*, 2023, pp. 4328–4338.

[28] T. Wang, B. Zhang, T. Zhang, S. Gu, J. Bao, T. Baltrusaitis, J. Shen, D. Chen, F. Wen, Q. Chen *et al.*, "Rodin: A generative model for sculpting 3d digital avatars using diffusion," in *CVPR*, 2023, pp. 4563–4573.

[29] Z. Zhao, W. Liu, X. Chen, X. Zeng, R. Wang, P. Cheng, B. Fu, T. Chen, G. Yu, and S. Gao, "Michelangelo: Conditional 3d shape generation based on shape-image-text aligned latent representation," *arXiv preprint arXiv:2306.17115*, 2023.

[30] J. Tang, Z. Chen, X. Chen, T. Wang, G. Zeng, and Z. Liu, "Lgm: Large multi-view gaussian model for high-resolution 3d content creation," *arXiv preprint arXiv:2402.05054*, 2024.

[31] M. Liu, C. Xu, H. Jin, L. Chen, Z. Xu, H. Su *et al.*, "One-2-3-45: Any single image to 3d mesh in 45 seconds without per-shape optimization," *arXiv preprint arXiv:2306.16928*, 2023.

[32] M. Liu, R. Shi, L. Chen, Z. Zhang, C. Xu, X. Wei, H. Chen, C. Zeng, J. Gu, and H. Su, "One-2-3-45++: Fast single image to 3d objects with consistent multi-view generation and 3d diffusion," *arXiv preprint arXiv:2311.07885*, 2023.

[33] Z.-X. Zou, Z. Yu, Y.-C. Guo, Y. Li, D. Liang, Y.-P. Cao, and S.-H. Zhang, "Triplane meets gaussian splatting: Fast and generalizable single-view 3d reconstruction with transformers," *arXiv preprint arXiv:2312.09147*, 2023.

[34] Z. Wang, Y. Wang, Y. Chen, C. Xiang, S. Chen, D. Yu, C. Li, H. Su, and J. Zhu, "Crm: Single image to 3d textured mesh with convolutional reconstruction model," *arXiv preprint arXiv:2403.05034*, 2024.

[35] B. Mildenhall, P. P. Srinivasan, M. Tancik, J. T. Barron, R. Ramamoorthi, and R. Ng, "Nerf: Representing scenes as neural radiance fields for view synthesis," *Communications of the ACM*, vol. 65, no. 1, pp. 99–106, 2021.

[36] T. Müller, A. Evans, C. Schied, and A. Keller, "Instant neural graphics primitives with a multiresolution hash encoding," *ACM Transactions on Graphics (ToG)*, vol. 41, no. 4, pp. 1–15, 2022.

[37] B. Kerbl, G. Kopanas, T. Leimkühler, and G. Drettakis, "3d gaussian splatting for real-time radiance field rendering," *ACM Transactions on Graphics*, vol. 42, no. 4, 2023.

[38] Y. Liu, C. Lin, Z. Zeng, X. Long, L. Liu, T. Komura, and W. Wang, "Syncdreamer: Generating multiview-consistent images from a single-view image," *arXiv preprint arXiv:2309.03453*, 2023.

[39] X. Long, Y.-C. Guo, C. Lin, Y. Liu, Z. Dou, L. Liu, Y. Ma, S.-H. Zhang, M. Habermann, C. Theobalt *et al.*, "Wonder3d: Single image to 3d using cross-domain diffusion," *arXiv preprint arXiv:2310.15008*, 2023.

[40] Y. Lu, J. Zhang, S. Li, T. Fang, D. McKinnon, Y. Tsin, L. Quan, X. Cao, and Y. Yao, "Direct2. 5: Diverse text-to-3d generation via multi-view 2.5 d diffusion," *arXiv preprint arXiv:2311.15980*, 2023.

[41] Z. Chen, Y. Wang, F. Wang, Z. Wang, and H. Liu, "V3d: Video diffusion models are effective 3d generators," *arXiv preprint arXiv:2403.06738*, 2024.

[42] Y. Shi, P. Wang, J. Ye, M. Long, K. Li, and X. Yang, "Mvdream: Multi-view diffusion for 3d generation," *arXiv preprint arXiv:2308.16512*, 2023.

[43] stability.ai, "Stable zero123," 2023, https://stability.ai/news/stable-zero123-3d-generation.

[44] P. Wang and Y. Shi, "Imagedream: Image-prompt multi-view diffusion for 3d generation," *arXiv preprint arXiv:2312.02201*, 2023.

[45] A. Radford, J. W. Kim, C. Hallacy, A. Ramesh, G. Goh, S. Agarwal, G. Sastry, A. Askell, P. Mishkin, J. Clark, G. Krueger, and I. Sutskever, "Learning transferable visual models from natural language supervision," 2021.

[46] L. Liu, Y. Ren, Z. Lin, and Z. Zhao, "Pseudo numerical methods for diffusion models on manifolds," *arXiv preprint arXiv:2202.09778*, 2022.

[47] F. Bao, C. Li, J. Zhu, and B. Zhang, "Analytic-DPM: an analytic estimate of the optimal reverse variance in diffusion probabilistic models," in *International Conference on Learning Representations*, 2022.

[48] F. Bao, C. Li, J. Sun, J. Zhu, and B. Zhang, "Estimating the optimal covariance with imperfect mean in diffusion probabilistic models," *arXiv preprint arXiv:2206.07309*, 2022.

[49] C. Lu, Y. Zhou, F. Bao, J. Chen, C. Li, and J. Zhu, "Dpm-solver: A fast ode solver for diffusion probabilistic model sampling in around 10 steps," in *Advances in Neural Information Processing Systems*, 2022.

[50] ——, "Dpm-solver++: Fast solver for guided sampling of diffusion probabilistic models," *arXiv preprint arXiv:2211.01095*, 2022.

[51] W. Zhao, L. Bai, Y. Rao, J. Zhou, and J. Lu, "Unipc: A unified predictor-corrector framework for fast sampling of diffusion models," *arXiv preprint arXiv:2302.04867*, 2023.

[52] J. Song, C. Meng, and S. Ermon, "Denoising diffusion implicit models," *arXiv preprint arXiv:2010.02502*, 2020.

[53] C. Lu, K. Zheng, F. Bao, J. Chen, C. Li, and J. Zhu, "Maximum likelihood training for score-based diffusion odes by high order denoising score matching," in *International Conference on Machine Learning*. PMLR, 2022, pp. 14 429–14 460.

[54] S. Nie, H. A. Guo, C. Lu, Y. Zhou, C. Zheng, and C. Li, "The blessing of randomness: Sde beats ode in general diffusion-based image editing," *arXiv preprint arXiv:2311.01410*, 2023.

[55] A. Q. Nichol and P. Dhariwal, "Improved denoising diffusion probabilistic models," in *International Conference on Machine Learning*. PMLR, 2021, pp. 8162–8171.

[56] Y.-C. Guo, Y.-T. Liu, C. Wang, Z.-X. Zou, G. Luo, C.-H. Chen, Y.-P. Cao, and S.-H. Zhang, "threestudio: A unified framework for 3d content generation," https://github.com/threestudio-project/threestudio, 2023.

[57] W. E. Lorensen and H. E. Cline, "Marching cubes: A high resolution 3d surface construction algorithm," in *Seminal graphics: pioneering efforts that shaped the field*, 1998, pp. 347–353.

[58] F. Liu, D. Wu, Y. Wei, Y. Rao, and Y. Duan, "Sherpa3d: Boosting high-fidelity text-to-3d generation via coarse 3d prior," *arXiv preprint arXiv:2312.06655*, 2023.

[59] L. Qiu, G. Chen, X. Gu, Q. Zuo, M. Xu, Y. Wu, W. Yuan, Z. Dong, L. Bo, and X. Han, "Richdreamer: A generalizable normal-depth diffusion model for detail richness in text-to-3d," *arXiv preprint arXiv:2311.16918*, 2023.

[60] R. Wu, B. Mildenhall, P. Henzler, K. Park, R. Gao, D. Watson, P. P. Srinivasan, D. Verbin, J. T. Barron, B. Poole *et al.*, "Reconfusion: 3d reconstruction with diffusion priors," *arXiv preprint arXiv:2312.02981*, 2023.

[61] L. Yariv, O. Puny, N. Neverova, O. Gafni, and Y. Lipman, "Mosaic-sdf for 3d generative models," *arXiv preprint arXiv:2312.09222*, 2023.

[62] J. Xu, W. Cheng, Y. Gao, X. Wang, S. Gao, and Y. Shan, "Instantmesh: Efficient 3d mesh generation from a single image with sparse-view large reconstruction models," *arXiv preprint arXiv:2404.07191*, 2024.

[63] Y. Wang, W. Lira, W. Wang, A. Mahdavi-Amiri, and H. Zhang, "Slice3d: Multi-slice, occlusion-revealing, single view 3d reconstruction," *arXiv preprint arXiv:2312.02221*, 2023.

[64] Y. Lan, F. Hong, S. Yang, S. Zhou, X. Meng, B. Dai, X. Pan, and C. C. Loy, "Ln3diff: Scalable latent neural fields diffusion for speedy 3d generation," *arXiv preprint arXiv:2403.12019*, 2024.

[65] D. Tochilkin, D. Pankratz, Z. Liu, Z. Huang, , A. Letts, Y. Li, D. Liang, C. Laforte, V. Jampani, and Y.-P. Cao, "Triposr: Fast 3d object reconstruction from a single image," *arXiv preprint arXiv:2403.02151*, 2024.

[66] M. Deitke, D. Schwenk, J. Salvador, L. Weihs, O. Michel, E. VanderBilt, L. Schmidt, K. Ehsani, A. Kembhavi, and A. Farhadi, "Objaverse: A universe of annotated 3d objects," in *CVPR*, 2023, pp. 13 142–13 153.

[67] M. Deitke, R. Liu, M. Wallingford, H. Ngo, O. Michel, A. Kusupati, A. Fan, C. Laforte, V. Voleti, S. Y. Gadre *et al.*, "Objaverse-xl: A universe of 10m+ 3d objects," *arXiv preprint arXiv:2307.05663*, 2023.

[68] Z. He and T. Wang, "Openlrm: Open-source large reconstruction models," https://github.com/3DTopia/OpenLRM, 2023.

[69] J. Li, H. Tan, K. Zhang, Z. Xu, F. Luan, Y. Xu, Y. Hong, K. Sunkavalli, G. Shakhnarovich, and S. Bi, "Instant3d: Fast text-to-3d with sparse-view generation and large reconstruction model," *arXiv preprint arXiv:2311.06214*, 2023.

[70] Y. Song, P. Dhariwal, M. Chen, and I. Sutskever, "Consistency models," in *International Conference on Machine Learning*. PMLR, 2023, pp. 32 211–32 252.

[71] S. Luo, Y. Tan, L. Huang, J. Li, and H. Zhao, "Latent consistency models: Synthesizing high-resolution images with few-step inference," *arXiv preprint arXiv:2310.04378*, 2023.

[72] T. Yin, M. Gharbi, R. Zhang, E. Shechtman, F. Durand, W. T. Freeman, and T. Park, "One-step diffusion with distribution matching distillation," *arXiv preprint arXiv:2311.18828*, 2023.

[73] A. Sauer, D. Lorenz, A. Blattmann, and R. Rombach, "Adversarial diffusion distillation," *arXiv preprint arXiv:2311.17042*, 2023.

[74] J. Ho and T. Salimans, "Classifier-free diffusion guidance," *arXiv preprint arXiv:2207.12598*, 2022.

[75] D. P. Kingma and M. Welling, "Auto-encoding variational bayes," *stat*, vol. 1050, p. 1, 2014.

[76] A. Van Den Oord, O. Vinyals *et al.*, "Neural discrete representation learning," *Advances in neural information processing systems*, vol. 30, 2017.

[77] C. Schuhmann, R. Beaumont, R. Vencu, C. W. Gordon, R. Wightman, M. Cherti, T. Coombes, A. Katta, C. Mullis, M. Wortsman, P. Schramowski, S. R. Kundurthy, K. Crowson, L. Schmidt, R. Kaczmarczyk, and J. Jitsev, "LAION-5b: An open large-scale dataset for training next generation image-text models," in *Thirty-sixth Conference on Neural Information Processing Systems Datasets and Benchmarks Track*, 2022. [Online]. Available: https://openreview.net/forum?id=M3Y74vmsMcY

[78] M. Cherti, R. Beaumont, R. Wightman, M. Wortsman, G. Ilharco, C. Gordon, C. Schuhmann, L. Schmidt, and J. Jitsev, "Reproducible scaling laws for contrastive language-image learning," *arXiv preprint arXiv:2212.07143*, 2022.

A Key hyperparameters of MicroDreamer

Table 1: **Key hyperparameters of MicroDreamer on three base diffusion models**. All models are employed to generate NeRF and the last two are employed to generate 3DGS and mesh. The hyperparameters are shared across the two settings by default. Otherwise, those for 3DGS are shown in brackets. T is end time of diffusion.

Model Select	**MVDream** [42]	**Stable Zero123** [6, 43]	**ImageDream** [44]
Diffusion			
CFG [74]	7.5	3.0	3.0 (2.0)
Forward process	hybrid	hybrid	hybrid (random noise only)
Time schedule of t_2	$0.8T \rightarrow 0.5T$	$0.8T \rightarrow 0.2T$	$0.8T \rightarrow 0.6T$ ($0.8T \rightarrow 0.4T$)
Sampling process	DDIM, $\eta = 0.0$	DDIM, $\eta = 0.5$	DDIM, $\eta = 1.0$
Discretization steps	50	20	10
3D training			
Resolution	$64 \rightarrow 128$	$64 \rightarrow 128 \rightarrow 196$ (256)	$64 \rightarrow 128$ (256)
Background	learned by NN	always white	always white
# camera views	4	4 (6)	4
# initialized steps	50	15	50
# iterations K	50	30 (20 or 30)	30
# reconstuction steps $I^{(k)}$	15	15	15
Loss type	ℓ_1	ℓ_1	ℓ_1
Reference color loss	-	0.1 (0.3)	0
Reference opacity loss	-	0.001 (0.01)	0

B The impact of latent diffusion model on 3D generation

Instead of applying the diffusion model directly in the pixel space to generate images, existing research [17] tends to use a VAE [75, 76] encoder to compress high-dimensional image data into a low-dimensional latent space first. Then a diffusion process is employed within this latent space to generate new images, which are finally decoded back by a VAE decoder to the pixel space to achieve high-quality images. We refer to this type of diffusion model as the latent diffusion model (LDM). The framework of LDM is adopted widely [6, 42, 44, 43], which leads to a significant impact on 3D generation.

B.1 SIR enabling optimization in the pixel space

Within the framework of LDM [17], the rendered images are mapped through an encoder $\mathcal{E}$ [75, 76] to a latent space, where the loss function is calculated. Consequently, the gradients must be propagated back through the encoder, further reducing the efficiency of 3D object generation. In such a case, the SIR loss in the latent space is given by:

$$\mathcal{J}_{\text{SIR-latent}}(\theta; c^{(k)}, \hat{x}^{(k)}) = \|\mathcal{E}(g(\theta, c^{(k)})) - \hat{x}^{(k)}\|. \tag{11}$$

An alternative approach maps the diffusion output back to the pixel space via the corresponding decoder $\mathcal{D}$, allowing for a similar loss function to be defined directly in pixel space. This method enables direct updates to 3D parameters without passing gradients through the encoder, thus enhancing efficiency.

However, we argue that this is not feasible for existing optimization methods [1, 2, 8] such as SDS. Even reparameterized as the data predicting form in Eq. (6), the pixel-level quality of the images obtained by SDS is poor for 3D optimization (see Appendix B.2). In contrast, SIR achieves higher quality generation results through a carefully designed refinement process, thereby enabling optimization in pixel space. The SIR loss in the pixel space is formalized as:

$$\mathcal{J}_{\text{SIR-pixel}}(\theta; c^{(k)}, \hat{x}^{(k)}) = \|g(\theta, c^{(k)}) - \mathcal{D}(\hat{x}^{(k)})\|, \tag{12}$$

which is about 2-3 times faster than Eq. (11) for 3D parameter optimization, as the ablation results shown in Fig. 8. It is set as the default loss throughout the paper.
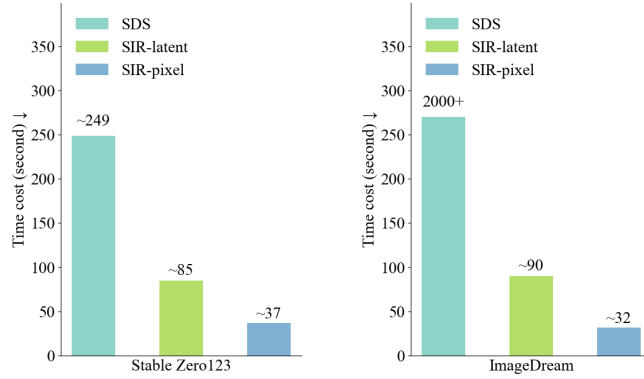
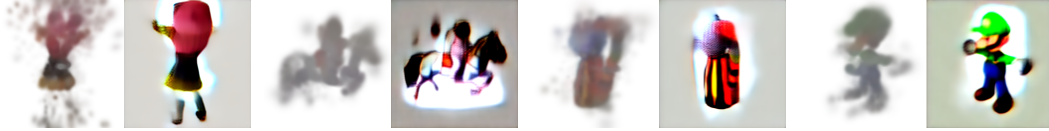Figure 8: Optimization in pixel space accelerates generation.

Figure 9: **Results of single-step prediction.** For each pair of images, the left is the input image and the right is the output of single-step prediction. The poor quality of the output makes it unsuitable for 3D optimization.

B.2 Faliure of applying SDS in pixel space.

We highlight that SDS optimizing in pixel space can not be effective even if it has the data predicting form by reparameterized as presented in Eq. (6). Fig. 9 shows the poor quality for single-step prediction from the diffusion model using Eq. (2). Therefore, if we attempt to employ SDS for optimization in the pixel space, i.e. optimizing 3D objects with 2D images like those generated in Fig. 9, the resulting 3D content would be of subpar quality, as the results presented in Fig. 10.
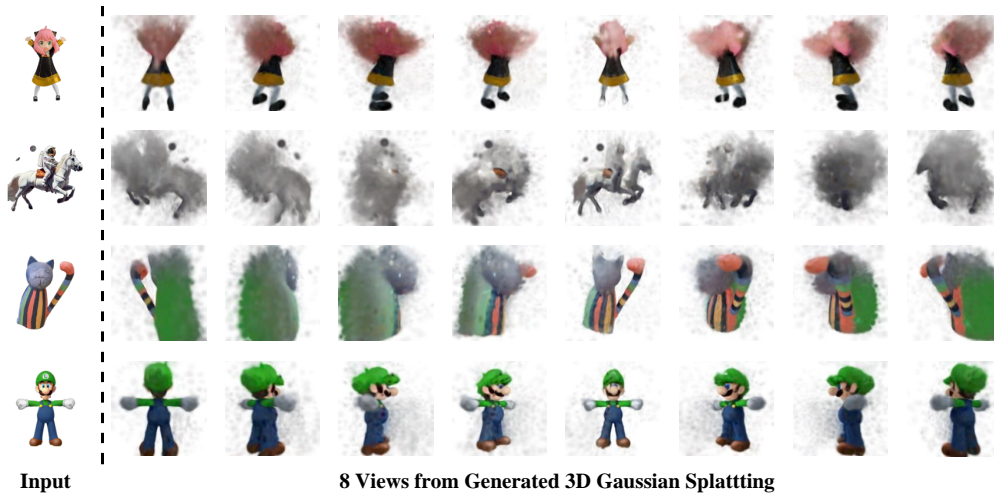

Input   **8 Views from Generated 3D Gaussian Splattting**

Figure 10: **Results of applying SDS in pixel space.** SDS optimizing in pixel space can not be effective.

Input   **8 Views from Generated 3D Gaussian Splattting**

Figure 11: **Results of SIR based on ImageDream on 3DGS.** These results images are rendered from 3DGS with no refinement stage.

Table 2: **Codebase.** URL and licenses are provided for the open-source assets we used in this paper.

Asset	URL	License
[56]	https://github.com/threestudio-project/threestudio	Apache-2.0 license
[9]	https://github.com/dreamgaussian/dreamgaussian	MIT license
[45]	https://huggingface.co/laion/CLIP-ViT-bigG-14-laion2B-39B-b160k	MIT license
[42]	https://github.com/bytedance/MVDream-threestudio	Apache-2.0 license
[43]	https://huggingface.co/stabilityai/stable-zero123	Sai-nc-community
[44]	https://github.com/bytedance/ImageDream	Apache-2.0 license
[24]	https://github.com/openai/point-e	MIT license
[23]	https://github.com/openai/shap-e	MIT license
[31]	https://github.com/One-2-3-45/One-2-3-45	Apache-2.0 license
[33]	https://github.com/VAST-AI-Research/TriplaneGaussian	Apache-2.0 license
[39]	https://github.com/xxlong0/Wonder3D	AGPL-3.0 license
[30]	https://github.com/3DTopia/LGM	MIT license

C   Time schedule of t_1

The hyperparameter t_1 regulates the balance between inversion and noise-adding, which varies with different models. In our earlier exploration, we adopted $t_1 = t_2^2/T$ for SIR based on MVDream [42] and ImageDream [44] on NeRF, and $t_1 = 0.6t_2$ for SIR based on Stable Zero123 [43, 6] on both NeRF and 3DGS. Notably, SIR based on ImageDream on 3DGS opted for $t_1 = t_2$, i.e., adding noise for the forward process. As an advanced multi-view diffusion model, ImageDream can generate images with enhanced 3D consistency, obviating the need for inversion to maintain consistency. Fig. 11 shows some results of SIR on ImageDream on 3DGS using $t_1 = t_2$ schedule.

D   More implementation details

Codebase. For the implementation of SIR and SDS on NeRF, we choose the popularly used framework threestudio [56]. For the implementation of SIR on 3DGS, we follow the framework from DreamGaussian [9]. The checkpoint we chose for CLIP computation is `laion/CLIP-ViT-bigG-14-laion2B-39B-b160k` [45, 77, 78]. In Sec. 5.2, we compare Micro-Dreamer with seven competitive baselines by utilizing the official code released in GitHub. See Tab. 2 for details about the URL and licenses of the assets we used in this paper.

Table 3: **Quantitative comparisons.** In terms of CLIP similarity, MicroDreamer achieves an excellent balance between efficiency and effectiveness.

Method	CLIP-Similarity ↑	Generation time ↓	Extra refine time↓
Point-E	0.510	∼ 24s	-
Shap-E	0.616	∼ 5s	-
One-2-3-45	0.617	∼ 42s	-
Wonder3D	0.699	∼ 30s	∼ 140s
TriplaneGaussian	0.647	∼ 7s	-
LGM	0.716	∼ 3s	∼ 50s
DreamGaussian	0.698	∼ 30s	∼ 10s
DreamGaussian-300 iters	0.656	∼ 18s	∼ 10s
MicroDreamer-20 iters (**Ours**)	0.678	∼ 18s	∼ 4s
MicroDreamer-30 iters (**Ours**)	0.687	∼ 26s	∼ 4s

Details in metric.   All the results presented in Sec. 5.2 were on the mesh representation. As Triplane-Gaussian [33] has no official mesh export code, we apply the mesh exported code from LGM [30] for it. For extra refine time, we record the time of second stage refinement for MicroDreamer and DreamGaussian [9], the time of generating 3D from multi-view images for Wonder3D [39], and the time for meshing through a NeRF for LGM [30], respectively.

Data used in ablation study.   We chose seven images collected from the test dataset to perform our ablation study in Fig. 7 and Fig. 8. We will include these images in the submitted supplementary material.

Safeguards.   Our method, which requires no additional models and doesn't release any new pre-trained model, can ensure security due to the inherent safe configuration of the employed 2D multi-view diffusion models [42, 43, 44].

E   More results

Results on 3DGS.   We provide more results on mesh exported from 3DGS for MicroDreamer-20 iters in Fig. 12.

Results on NeRF.   In Fig. 13, we present a comparison of the generated quality between SIR and SDS on NeRF in the same short time under different base diffusion models [42, 43, 6, 44]. SIR can generate NeRF of high visual quality in a shorter time than SDS, as the results represented. Notably, SIR accelerates the generation process in ImageDream more, as it's an advanced multi-view diffusion model that can produce higher-quality multi-view images and support fewer discretization steps for the diffusion process, lowering NFEs.

Limitations.   In Fig. 14, we show some of the less successful cases generated by our method. Due to the limited ability of the diffusion model, inputs with complex geometric structures such as central hollowing may result in satisfactory mesh outcomes. Furthermore, existing diffusion models struggle to generate the rear view of an object, which often leads to poorly textured back surfaces of the generated meshes. These problems may be solved as the quality of the images the multi-view diffusion model generated improves.

F   Quantative comparison on 3DGS

We provide the detailed quantitative comparison table in Tab. 3. For a fair comparison, we also explored the performance of DreamGaussian with fewer iterations (300 iterations) whose generation time is near MicroDreamer-30 iters. As shown in Tab. 3, MicroDreamer performs better than DreamGaussian over a similar amount of time, further illustrating that MicroDreamer attains a commendable efficiency-performance balance.
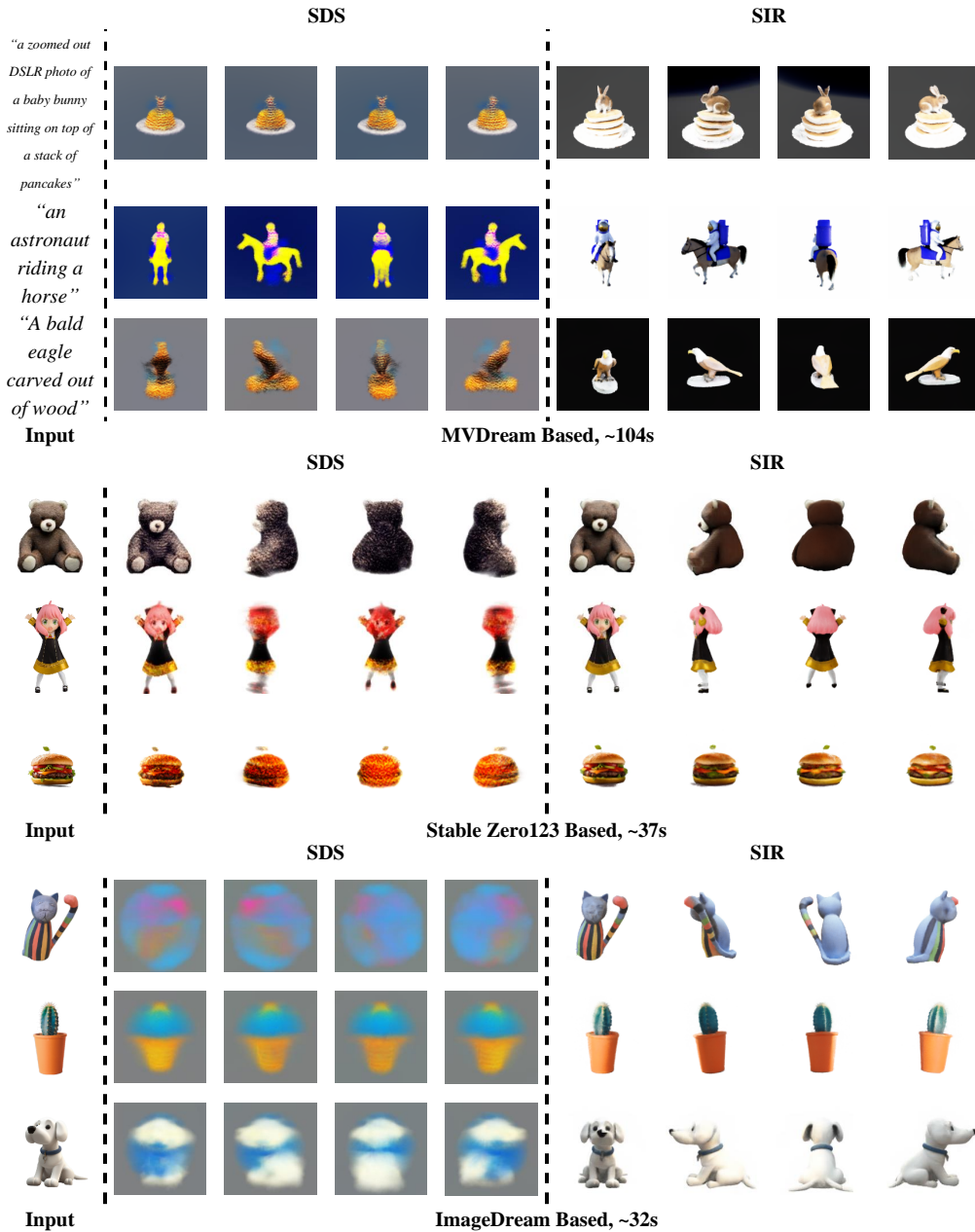
Figure 12: More results for MicroDreamer-20 iters.

Figure 13: **Comparison of the generated quality between SIR and SDS in the same short time on NeRF.** SIR can generate NeRF of high visual quality in less time than SDS.
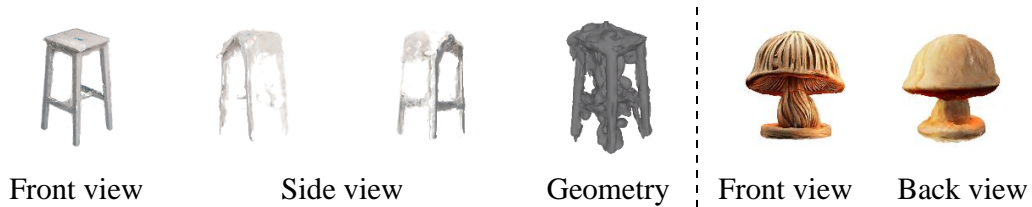

Figure 14: **Limitations.** Visualization of some less satisfactory cases generated by our methods.